# Finite-Gain Repetitive Controller for Harmonic Sharing Improvement in a VSM Microgrid

Roldán-Pérez, J.; Prodanovic, Momcilo; Rodríguez-Cabero, A.; Guerrero, J. M.; García-Cerrada, A.

*Published in:*
IEEE Transactions on Smart Grid

*DOI (link to publication from Publisher):*
10.1109/TSG.2019.2913632

*Publication date:*
2019

*Document Version*
Accepted author manuscript, peer reviewed version

# Finite-Gain Repetitive Controller for Harmonic Sharing Improvement in a VSM Microgrid

J. Roldán-Pérez, *Member, IEEE*, M. Prodanovic, *Member, IEEE*, A. Rodríguez-Cabero, J. M. Guerrero, *Fellow, IEEE*, and A. García-Cerrada, *Senior Member, IEEE*

***Abstract*—Electronic power interfaces are commonly used in microgrids for renewable energy integration and a control method based on a Virtual Synchronous Machine (VSM) represents an attractive alternative to conventional approaches. This control method has several advantages, however, a number of issues still need to be properly addressed, including those of power quality and harmonic current sharing. In this paper, a Finite-Gain Repetitive Controller (FGRC) is proposed to improve current harmonic distribution in microgrids based on VSMs. Stability, transient performance and performance under frequency variations are studied analytically. When compared to other control options, the method proposed here is capable of dealing with all harmonics simultaneously. A comparative analysis is provided to emphasise the contributions of this work. The control system improvements were tested on a prototype microgrid consisting of two 15 kVA VSMs, distribution line impedances and a non-linear load.**

***Keywords*—Virtual Synchronous Machine, Microgrid, Power Quality, Repetitive Controller, Harmonic Sharing.**

## I. Introduction

In recent years, renewable energy sources have drawn much attention and microgrid environments are frequently used for their integration and operation. These energy sources are typically connected to microgrids by using droop-controlled electronic power converters and the droop control itself has been studied in depth in [1, 2]. However, an alternative way to integrate converters to microgrids is the emulation of a synchronous machine to create what is commonly known in the literature as Virtual Synchronous Machines (VSMs) [3], Virtual Synchronous Generators (VSGs) [4], or synchronverters [5].

The method of emulation of synchronous machines requires more research efforts in order to find solution for several implementation issues such as voltage and current limiting [6], operation under voltage sags [7] and under distorted grid conditions [8]. Current limiting was studied by Hirase *et al.* [9], where an internal current controller for a VSM was proposed. The reference current was calculated by using a model of the connection filter. This concept was adapted for single-phase inverters by Younis *et al.* [10]. Alternative solutions can be found in the literature [11, 12]. Internal current controllers have also been proposed for Synchronous Power Controllers (SPCs) [13–16], representing an alternative to VSMs. Current limiting in VSMs generates additional problems related to angle stability [17] and it has been already addressed by modifying the virtual-shaft characteristics during large disturbances [18]. Operation of VSMs under distorted grid conditions is also an important issue, although it has been seldom studied [8]. In this paper, power quality aspects of VSMs in microgrids are addressed and the obtained improvements represent one of the contributions of this paper.

Power quality in microgrids has attracted attention of researchers because most electric loads consume non-sinusoidal currents that should be shared between Distributed Generators (DGs) [19]. However, in practical applications, the output impedances of DGs are not equal and loads are connected via distribution lines. These facts prevent the proportional distribution of harmonic currents. Power quality issues are often addressed by using the idea of a virtual impedance when controlling Voltage Source Converters (VSCs) in microgrid applications [20]. A detailed literature review of harmonic control in microgrids and the use of virtual impedances will be presented in Section II.

All the alternative solutions found in the literature for accurate harmonic sharing are based on resonant controllers. Repetitive controllers (RCs) have not been applied yet as virtual impedances. An RC has the advantage of dealing with "all" harmonics within its bandwidth whilst resonant controllers have to be tuned to specific known and present frequencies. However, an RC does not allow independent tuning for each frequency unlike resonant controllers. RCs are used in power electronics applications such as active power filters [21]. They give infinite open-loop gain at harmonic frequencies and the design is straightforward [21]. However, RCs are sensitive to changes in the grid frequency and microgrids are prone to transient frequency variations. Although several solutions have already been proposed to provide infinite gain at harmonic frequencies despite frequency variations [22–25], the use of an RC as a virtual impedance requires high (but not infinite) gain at the harmonic frequencies and this is addressed in detail in this paper. In some occasions, the gain of RCs is limited in order to avoid stability problems. For example, an internal stability problem generated by the use of a RC in a DVR was solved in [23] by reducing the internal gain of the RC. In [26], the gain was reduced in order to limit the harmonics present in the command signal. Similar ideas can be found in the literature [27, 28]. In this paper the finite gain of the RC

J. Roldán-Pérez, M. Prodanovic, and A. Rodríguez-Cabero are with the Electrical Systems Unit, IMDEA Energy Institute. J. M. Guerrero is with Department of Energy Technology, Aalborg University. A. García-Cerrada is with Department of Electronics, Control Engineering and Communications, and with the Institute for Research in Technology, ICAI School of Engineering, Universidad Pontificia Comillas.

This work was supported in part by the Community of Madrid Government under the project PRICAM (S2013/ICE-2933). Corresponding author phone: +34917371120, e-mail: javier.roldan@imdea.org.

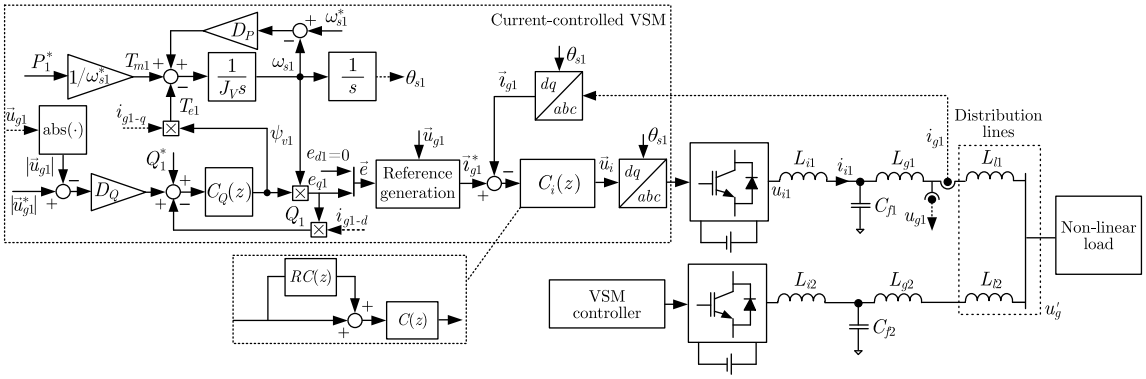


Fig. 1. Control and circuit diagram of a VSM-based microgrid with non-linear loads. VSMs include a current controller, where the FGRC is applied. The current controller consists of a main and a harmonic controller, called $C(z)$ and $RC(z)$, respectively.

is treated as a necessary feature to improve current harmonic sharing in a microgrid. It will be shown that by changing the RC amplification, the current harmonic distribution can be improved. This represents the main contribution of this paper.

In this paper, a Finite-Gain Repetitive Controller (FGRC) is proposed to adjust the output impedance of VSMs in microgrids so that current harmonics are correctly shared. A current-controlled version of VSMs has been used to make the application of an FGRC possible. It is shown that an FGRC provides adjustable gain at the harmonic frequencies and it is demonstrated that a current-controlled VSM with an FGRC is similar to a classical VSM with a harmonic virtual impedance. However, with an FGRC all harmonics are addressed at the same time and there is no need to add a resonator for each new harmonic that needs to be addressed. Transient performance, steady-state operation and stability are all studied in detail. The main contributions were validated on a prototype consisting of two 15 kVA VSMs feeding a non-linear load connected via configurable impedances. A short version of this paper was presented in a conference [29].

## II. Power Quality in Microgrids

Power quality issues in Uninterruptible Power Supply (UPS) systems and microgrids have already been studied in depth [30, 31]. Hardware solutions can be applied to accurately share current harmonics, although control techniques like the virtual impedance are most common in microgrid applications. An extensive literature review of virtual impedance applications can be found in [32]. Most authors apply resistive virtual impedances [33], although more advanced alternatives are also possible [8]. For example, Munir and Li [34] presented a virtual impedance for PV inverters in electrical distribution systems. The effect of capacitor banks used to compensate reactive power was explored and tips to improve power quality based on tuning the virtual impedances were provided. Chen *et al.* [35] presented a voltage controller for VSCs based on virtual impedances. Dead-time effects were analysed and a harmonic virtual impedance was proposed to improve current quality. Blanco *et al.* [36] presented the virtual-admittance concept for parallel-connected DGs in microgrids. Virtual admittances allowed current harmonics to be shared between voltage- and current-controlled DGs. Resistive virtual impedances based on lead-lag [37] or high-pass [38] filters are commonly applied for converters that operate in parallel connection. However, it is difficult to share current harmonics properly if there are long distribution lines and a classical virtual impedance is applied. In these cases solutions based on resonators are commonly adopted [39, 40].

Specific solutions to address harmonic issues based on resonant structures have already been studied in the literature. Ni. *et al.* [41] presented the control system for a current-source rectifier based on harmonic virtual impedances. The proposed controller was compared with the selective harmonic elimination (SHE) pulse-width modulation (PWM) method and the benefits of virtual impedances were highlighted. He *et al.* [42] presented a harmonic compensation method based on the Sliding Discrete Fourier Transform (DFT). Each harmonic was extracted and its virtual impedance tuned independently. Extensive analysis was carried out in order to highlight voltage and current quality trade-off. Tian *et al.* [43] presented a hybrid harmonic controller for DGs that used resonant current and voltage compensators to produce a tailored output impedance. This feature allowed a trade-off between current and voltage quality. He *et al.* [39] presented a dual converter that includes a virtual impedance to improve load- and current-harmonic sharing. Virtual impedances have been also applied to improve the output-current quality in parallel-connected VSMs [44].

An alternative to the virtual impedance approach is a secondary controller that sends harmonic references to DGs through a communication link to improve current harmonic distribution [45] or voltage quality in nodes across a microgrid [46]. However, wide-bandwidth communication links are required [45].

## III. Application and Control System Overview

### A. System Description and Control Structure

Fig. 1 shows the schematics of a microgrid based on VSMs. Each VSM is connected to the microgrid via an $LCL$ filter. The VSM is applied by using an indirect current controller [6, 18]. Variables related to a specific DG are noted with the DG number in the subscript (e.g. $i_{g1}$), but this number is omitted in the rest of the paper when not necessary. The converter-side current is $i_i$ and the grid-side current is $i_g$. The

converter-side inductor is $L_i$, $L_g$ is the grid-side inductor, $C_f$ is the filter capacitor, and $L_l$ is the line inductance. Copper losses of inductors and lines are modelled with $R_i$, $R_g$, and $R_l$, respectively. The VSM generates a voltage reference ($\vec{e}$) that is transformed to a fictitious current reference ($\vec{i}_g^*$). This reference is tracked by an internal current controller, which is divided into a main and a harmonic controller. The internal controller includes decoupling equations in order to control the dynamics of the $dq$ axis components, independently [21]. The main controller ($C(z)$) provides a fast transient response, while the harmonic controller ($RC(z)$) deals with harmonic issues. This paper shows that an FGRC inside the current controller has a performance like a harmonic virtual impedance applied to VSMs. The main tasks of the supplementary harmonic controller can be summarised as follows:

1) Current harmonics generated by loads should be proportionally shared between DGs.
2) Voltage quality in the microgrid nodes should be maximised.

These two requirements are contradictory and a virtual impedance can be used to adjust the trade-off between them. This paper demonstrates that an FGRC implemented inside a current control loop is an effective tool to adjust the aforementioned trade-off.

### B. VSM in a Synchronous Reference Frame (SRF)

This section summarizes the VSM formulation in a SRF [5, 47]. The VSM virtual shaft is given by

$$J_V \cdot d\omega_s/dt = T_m - T_e + D_T(\omega_s^* - \omega_s),\ d\theta_s/dt = \omega_s, \quad (1)$$

where $\theta_s$ is the virtual shaft angle, and $\omega_s$ and $\omega_s^*$ are the synchronous frequency and its set point, respectively. The virtual moment of inertia is $J_V$, $D_T$ combines damping and droop, while,

$$T_e = P/\omega_s = \psi_v i_{i-q},\ \ T_m = P^*/\omega_s \approx P^*/\omega_s^*, \quad (2)$$

where $\omega_s \approx \omega_s^*$ in steady state. If the damping provided by the coefficient $D_T$ is insufficient, additional terms can be introduced to the VSM formulation [4, 48]. The active power injected by the VSM is $P$, while $P^*$ is its set-point value. The VSM output voltage is $\vec{e} = e_d + je_q$, where $e_q = \psi_v\omega_s$ and $e_d = 0$. The signal $\psi_v$ is called virtual flux, and it is used to control the reactive power injected by the VSM:

$$\psi_v = K_Q \int (Q^* + Q_D^* - Q)\, dt, \quad (3)$$

where $Q^*$ is the reactive power set point and $K_Q$ is the reactive power controller gain. Grid voltage support is provided by using the following control law:

$$Q_D^* = D_Q(|\vec{u}_g^*| - |\vec{u}_g|), \quad (4)$$

where $D_Q$ is a droop coefficient, $|\vec{u}_g|$ is the grid voltage modulus and $|\vec{u}_g^*|$ is its set point.

Active and reactive powers are calculated with [47, 49]:

$$P = \omega_s\psi_v i_{i-q} \approx u_{g-d}i_{g-d} + u_{g-q}i_{g-q}, \quad (5)$$

$$Q = \omega_s\psi_v i_{i-d} \approx u_{g-q}i_{g-d} - u_{g-d}i_{g-q}, \quad (6)$$

where the $dq$ components of the signals involved are calculated by using the power-invariant Park's Transformation [49].

### C. Current-Controlled VSM

An indirect current controller for VSMs was proposed in [6] and it is used here to simplify the application of the FGRC. Indirect current controllers were previously proposed in the literature for VSMs [11, 12] and SPCs [15, 16]. The main idea can be explained as follows.

If the filtering capacitor is neglected, the steady-state equations of the connection filter are [18]:

$$\begin{bmatrix} e_d - u_{g-d} \\ e_q - u_{g-q} \end{bmatrix} = \begin{bmatrix} R_{ig} & -\omega_s L_{ig} \\ \omega_s L_{ig} & R_{ig} \end{bmatrix} \begin{bmatrix} i_{g-d} \\ i_{g-q} \end{bmatrix}, \quad (7)$$

where $L_{ig} = L_i + L_g$ and $R_{ig} = R_i + R_g$. This equation can be used to generate a fictitious current reference ($\vec{i}_g^*$):

$$\begin{bmatrix} i_{g-d}^* \\ i_{g-q}^* \end{bmatrix} = K_z \begin{bmatrix} R_{ig} & \omega_s^* L_{ig} \\ -\omega_s^* L_{ig} & R_{ig} \end{bmatrix} \begin{bmatrix} e_d - u_{g-d}^f \\ e_q - u_{g-q}^f \end{bmatrix}, \quad (8)$$

with

$$K_z = 1/(R_{ig}^2 + L_{ig}^2\omega_s^{*2}), \quad (9)$$

where $\vec{u}_g^f$ is a filtered version of $\vec{u}_g$. The block diagram of this control strategy is depicted in Fig. 1. The current controller includes a set of decoupling equations in order to control the dynamics of the $dq$ axes, independently.

### D. Current Harmonics in Microgrids

Current harmonic distribution between two VSCs in a microgrid can be studied with the equivalent circuit depicted in Fig. 2, where $G_L(z)$ is the equivalent discrete-time load admittance and $z$ is the transformation variable usually associated to discrete-time transfer functions or Z-transformed variables. $Z_1(z)$ and $Z_2(z)$ are the output impedances of $DG1$ and $DG2$, respectively. These two impedances are shaped by the converter closed-loop control systems. The ratio between each DG output current and the load current is

$$\frac{I_{g1}(z)}{I_L(z)} = \frac{1/Z_1(z)}{1/Z_1(z) + 1/Z_2(z) + G_L(z)} \quad (10)$$

and

$$\frac{I_{g2}(z)}{I_L(z)} = \frac{1/Z_2(z)}{1/Z_1(z) + 1/Z_2(z) + G_L(z)}. \quad (11)$$

If the DGs have the same rated power, the following relationship can be written

$$R(z) = I_{g1}(z)/I_{g2}(z) = Z_2(z)/Z_1(z), \quad (12)$$

where $R(z)$ will be called "harmonic-sharing ratio".

The frequency response of any discrete-time transfer function for any harmonic $h$ of a fundamental frequency $\omega_s$ ($h\omega_s$) can be calculated substituting $z$ by

$$z = \hat{\omega}_h = e^{j\omega_s h t_s}, \quad (13)$$

where $t_s$ is the sampling period and $\hat{\omega}_h^o$ refers to (13) calculated at the nominal frequency. A value of $|R(\hat{\omega}_h)|$ close to 1 leads to an equal distribution of the h-th harmonic current. If $|R(\hat{\omega}_h)| > 1$, DG1 will be absorbing a higher percentage of the h-th harmonic current (and vice-versa if $|R(\hat{\omega}_h)| < 1$).

This article has been accepted for publication in a future issue of this journal, but has not been fully edited. Content may change prior to final publication. Citation information: DOI 10.1109/TSG.2019.2913632, IEEE Transactions on Smart Grid



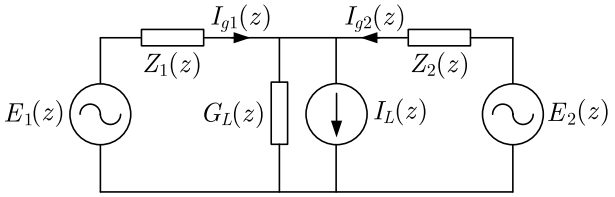


Fig. 2. Electrical circuit used to study harmonic distribution in microgrids.

### E. Virtual Impedance for VSMs

Virtual impedances are commonly applied to actively modify the output impedance of DGs. This modification is mainly applied to improve the power-flow control [33], but it can be also used to modify current harmonic distribution (see (12)) and this case will be studied in the paper [44].

Fig. 3 (a) shows the virtual impedance concept proposed for VSMs in [44]:

$$U_i(z) = E(z) - Z_v(z) I_g(z) = E(z) - Z_v(z) P(z) U_i(z), \quad (14)$$

where $E(z)$, $U_i(z)$, and $I_g(z)$ are the z-transformations of $e(t)$, $u_i(t)$, and $i_g(t)$, respectively. $P(z) = I_g(z)/U_i(z)$ is the plant discrete-time transfer function and $Z_v(z)$ is the virtual impedance.

In order to avoid interactions between the VSM and the harmonic virtual impedances, the output of the VSM ($\vec{e}$) is filtered by using notch filters. This guarantees that harmonics are not affected by the VSM dynamics [8].

## IV. Proposed Controller Configuration

This paper proposes an RC with a non-infinite gain (FGRC) as an alternative to resonant controllers [44] to shape a VSM's output impedance for harmonic components. An FGRC introduces a high gain at the fundamental frequency that would interact with the VSM's control system, but this issue can be solved by applying the indirect current controller explained in Section III-C. Within the current controller there is no problem with the high gain introduced by the RC at the fundamental frequency because the impedance at this frequency is not modified. However, although the virtual impedance concept cannot be directly applied since the controlled variable is $i_g$ instead of $e$, the control scheme in Fig. 3 (b) can be proposed to make this application possible [18]. In this control scheme, the z-domain transformation of the time-domain variables presented in Fig. 1 is used. The open-loop transfer function for the case in Fig. 3 (a) is

$$G(z) = Z_v(z) P(z), \quad (15)$$

while for the case in Fig. 3 (b) is (see Fig. 4)

$$G(z) = C_i(z) P(z) = (1 + RC(z)) C(z) P(z). \quad (16)$$

Without loss of generality, the set points for each of the control strategies can be written as

$$E(z) = \tilde{E}(z) + \bar{E}(z) \ \text{ and } \ I_g^*(z) = \tilde{I}_g^*(z) + \bar{I}_g^*(z), \quad (17)$$

where the tilde "˜" refers to the harmonic components and the bar "¯" refers to the fundamental component. The use

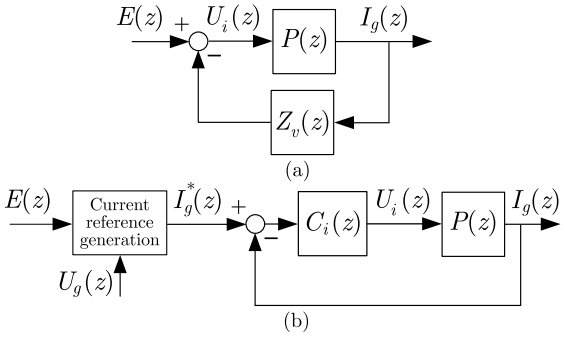


Fig. 3. Control diagram of a VSM with (a) a harmonic virtual impedance and (b) an indirect current controller.

of notch filters at the harmonic frequencies in the VSM [44] guaranteeds that $\tilde{E}(z) = 0$ for case (a), and $\tilde{I}_g^*(z) = 0$ for case (b). In this situation, any disturbance-to-output transfer function calculated with either Fig. 3 (a) or (b) have the same structure. By comparing (15) and (16), the equivalent virtual impedance for the case (b) can be written as:

$$Z_v^{eq}(z) = (1 + RC(z)) C(z). \quad (18)$$

Therefore, the equivalent virtual impedance can be modified by changing the amplification of $RC(z)$ and $C(z)$ at the harmonic frequencies (the placing of $RC(z)$ and $C(z)$ is shown in Fig. 1). The design and analysis of an FGRC applied to this scenario is addressed in detail here and represents the main contribution of this paper.

## V. Finite-Gain Repetitive Controller (FGRC)

### A. FGRC Fundamentals

The proposed controller is depicted in Fig. 4, where $RC(z)$ is the discrete-time FGRC, $G_p(z) = C(z)P(z)$ is the open-loop plant, and $Q(z)$ is a low-pass filter that limits the bandwidth. The transfer function $G_x(z)$ and the gain $K_x$ are used to guarantee closed-loop stability [21]. $K_o$ is used to adjust the FGRC gain at the harmonic frequencies and it is explained in Section V-B. This controller configuration is commonly known as "plug-in", and its main advantage is that the RC sees a plant where the effects such as resonances and delays have already been dealt with by the main controller [21].

In order to track even harmonics in *dq* (only):

$$W(z) = z^{-N/2} L(z), \quad (19)$$

where $L(z)$ is a filter that improves the FGRC performance under frequency deviations and $N/2$ is the number of single-period delays in the FGRC. The fundamental period of the disturbance is $t_p$.

The fundamental frequency of the microgrid ($\omega_s$) will vary according to the load because of the active-power droop coefficients included in the VSMs. Therefore, in order to provide frequency adaptation, $t_p$ is divided as follows [23]:

$$t_p = N t_s + l_e t_s, \quad (20)$$

where

$$N/2 = t_s/(t_p/2) \in \mathbb{N} \ \text{ and } \ l_e \in [0, 1). \quad (21)$$

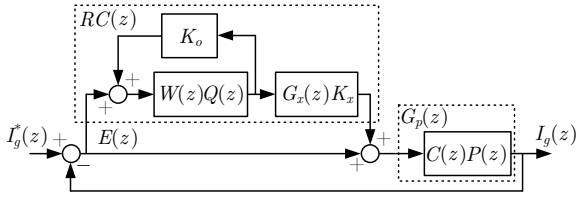


Fig. 4. Block diagram of a Finite-Gain Repetitive Controller (FGRC).

In (21), $N/2$ represents the number of integer delays, while $l_e$ is the fractional part of a delay that cannot be directly discretized and, therefore, it should be approximated. There are several alternatives to design the filter $L(z)$. In this paper, a first-order all-pass filter is applied [23]:

$$L(z) = \frac{(1-l_e) + (1+l_e)\, z^{-1}}{(1+l_e) + (1-l_e)\, z^{-1}}. \tag{22}$$

Therefore, the values of $N$ and $l_e$ change with the VSM synchronous frequency ($\omega_s$). The stability of RCs under fast variations of $N$ was studied by Olm *et al.* [50]. However, in this work $N$ and $l_e$ are calculated using the filtered version of the VSM frequency ($\omega_s^f$). Therefore, the adaptation mechanism does not interact with the rest of the control system dynamics. Under nominal conditions, $t_p = 1/(2\pi\omega_s^o)$, where $\omega_s^o$ is the nominal frequency of the grid. The FGRC transfer function is:

$$RC(z) = \frac{W(z)Q(z)}{1 - K_o W(z)Q(z)} G_x(z) K_x. \tag{23}$$

### B. FGRC Stability Analysis

From Fig. 4, the reference-to-error transfer function is:

$$F_e(z) = \frac{1}{1+G_p(z)} \overbrace{\frac{1 - K_o W(z)Q(z)}{1 - W(z)Q(z)(K_o - K_x G_x(z) F_p(z))}}^{S(z)} \tag{24}$$

where:

$$F_p(z) = G_p(z)/(1+G_p(z)), \tag{25}$$

is the closed-loop plant. A sufficient condition to guarantee closed-loop stability can be obtained by applying the small-gain theorem to the system in (24) [51], yielding

$$||W(z)Q(z)(K_o - K_x G_x(z) F_p(z))||_\infty < 1, \tag{26}$$

with $z = e^{j\omega t_s}$. The transfer function $G_x(z)$ is chosen as:

$$G_x(z) = \hat{F}_p^{-1}(z), \tag{27}$$

in order to fulfil the stability condition in (26), where $\hat{F}_p(z)$ is a model of $F_p(z)$ [21].

The filter $Q(z)$ limits FGRC bandwidth, and it is chosen as follows:

$$Q(z) = \sum_{k=-Q}^{Q} a_k z^k, \;\; a_{-k} = a_k, \tag{28}$$

where $a_k$ are the filter coefficients and $(2Q+1)$ is the filter size. The coefficients can be designed using several methods. In this paper, a $\mathrm{sinc}(\cdot)$ function filtered with a Hamming window in the frequency domain has been used (see [52], Section 5.3.2 for more details)

Within the FGRC bandwidth, $|Q(e^{j\omega t_s})| \approx 1$, while $|Q(e^{j\omega t_s})| \approx 0$ out of it. Therefore, within the bandwidth, the stability condition in (26) is reduced to

$$|K_o - K_x| < 1, \tag{29}$$

which is valid for any configuration of $W(z)$ provided that $|W(e^{j\omega t_s})| \leq 1 \;\forall\omega$ (always the case in this paper). The effect of $K_o$ will be investigated in Section VI. Meanwhile, the maximum value of $K_x$ that leads to a stable system can be obtained by solving (29),

$$0 < K_x < 1 + K_o, \tag{30}$$

if $K_o > 0$. The smaller $K_o$ is, the smaller the maximum value of $K_x$ becomes. $K_o$ and $K_x$ set the equivalent virtual impedance and their design is addressed in Section VI-A.

## VI. FGRC Design Considerations

### A. Equivalent Virtual Impedance

The equivalent harmonic virtual impedance value can be obtained by substituting $z = \hat{\omega}_h$ in $Z_v^{eq}(z)$ in (18), yielding

$$R_h = |Z_v^{eq}(\hat{\omega}_h)| = \frac{1 - K_o + K_x}{1 - K_o} \cdot |C(\hat{\omega}_h)| \cdot |G_x(\hat{\omega}_h)|. \tag{31}$$

The value of $R_h$ can be chosen by modifying either $K_o$ or $K_x$. However, it also depends on $|C(\hat{\omega}_h)|$ and $|G_x(\hat{\omega}_h)|$. The value of $K_o$ will be chosen according to the bandwidth requirements. Meanwhile, $R_h$ will be set according to the harmonic sharing needs. Therefore, the value of $K_x$ is fixed and it can be calculated from (31),

$$K_x = (1 - K_o) R'_h / (|C(\hat{\omega}_{h'})| \cdot |G_x(\hat{\omega}_{h'})|) - 1 + K_o, \tag{32}$$

where $h'$ is one of the harmonic frequencies. Equation (32) shows that the virtual impedance can be set, exactly, only for a given harmonic $h'$. In addition, $K_x$ must comply with the stability condition in (30). Otherwise, either $R'_h$ or (preferably) $K_o$ should be modified. The gain at different harmonic frequencies can be modified if the amplification of $Q(z)$ changes with frequency. This case will not be studied in this paper, but it is of interest for further research.

Fig. 5 shows the frequency response of $1 + RC(z)$ when the value of $K_o$ is modified and $K_x$ is adjusted with (32) so that the virtual resistance ($R_h$) is 10 dB, always. The lower the value of $K_o$, the more robust the system becomes against frequency variations. However, stability margins deteriorate because $K_x$ is closer to its limits. $K_o$ could be set to zero but this is not recommended because it would lead to a very narrow range for the selection of $K_x$.

### B. Performance with Frequency Variations

If $t_p$ (period of the grid frequency) varies during operation, the FGRC will be detuned and this will modify the equivalent impedance for harmonic frequencies. This effect can be quantified with [23]:

$$|F_e(e^{j\omega_s^o(1+\delta\omega_s)ht_s})|, \;\forall h \in \mathrm{H}, \tag{33}$$

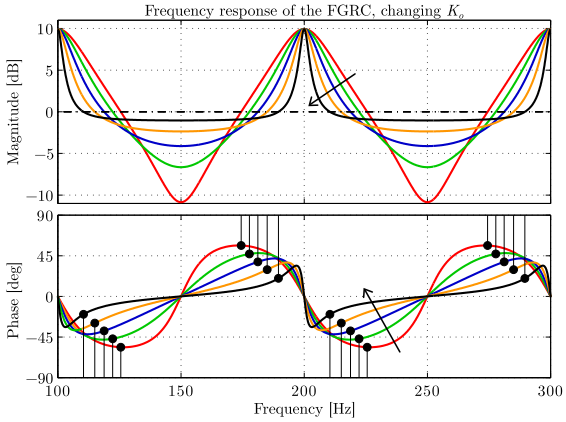


Fig. 5. Bode diagram of $1 + RC(z)$, for $K_o$ =0.5, 0.6, 0.7, 0.8, and 0.9 (increasing direction of the arrow). $R_h = 10$ dB. Black dots indicate where phase margins can be calculated. The arrow indicate the increasing direction of $K_o$.

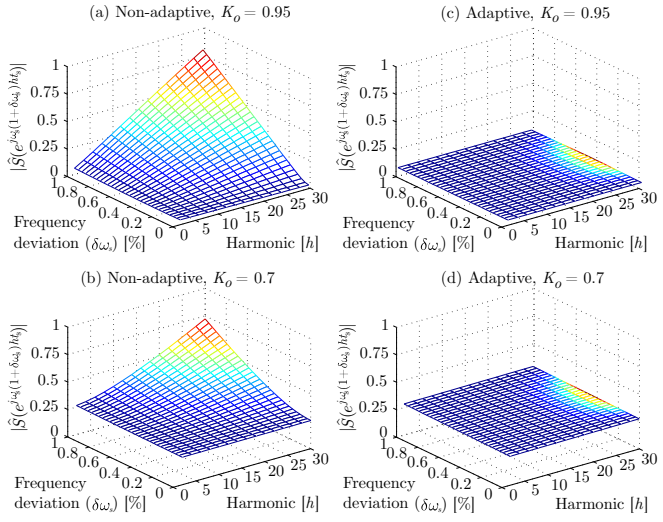


Fig. 6. Performance of the FGRC (left) excluding and (right) including $L(z)$. (top) $K_o = 0.95$ and (bottom) $K_o = 0.7$.

where

$$\delta\omega_s = (\omega_s - \omega_s^o)/\omega_s^o \tag{34}$$

is the frequency deviation in per-unit (50 Hz is the base value) values and H includes all the harmonics within the RC bandwidth. To facilitate interpretation, it is common to analyse $S(z)$ instead of $F_e(z)$ because the former does not depend on the plant. Also, it is commonly assumed that $F_p(z)G_x(z) = 1$ (perfect model of the plant) and $Q(z) = 1$ (operation within the bandwidth), yielding,

$$\hat{S}(z) = \frac{1 - K_o W(z)}{1 - W(z)(K_o - K_x)}, \tag{35}$$

where $\hat{S}(z)$ is a simplified version of $S(z)$.

Fig. 6 (left) shows the value of $|\hat{S}(e^{\omega_s(1+\delta\omega_s)ht_s})|$ for the FGRC when the grid frequency varies and no frequency adaptation method is applied. In (a) $K_o = 0.95$ and in (b) $K_o = 0.7$, while $K_x = 1$. In both cases, the error increases when the frequency varies. However, the reduction $K_o$ improves robustness against frequency variations. Fig. 6 (left) shows the same analysis, but including $L(z)$. Robustness against frequency variations improves, but real-time adaptation is required. These results indicate that filter $L(z)$ can be removed for moderate frequency variations if the value of $K_o$ is adjusted properly.

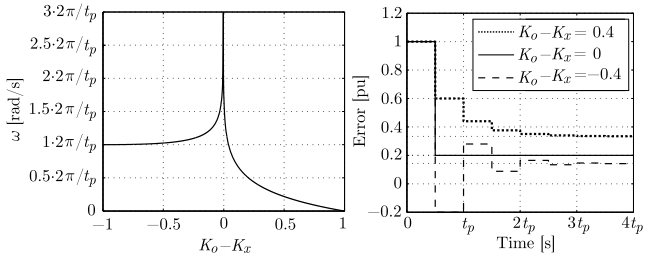


Fig. 7. (left) Frequency of the smallest pole (continuous-time domain) by changing $(K_o - K_x)$. (right) Transient response of $\hat{S}(z)$ for different values of $(K_o - K_x)$, with $K_o = 0.8$.

### C. FGRC Transient Performance

The transient response of the closed-loop system can assessed with the poles of $\hat{S}(z)$. Since the transient response of the FGRC will be slower than that of the plant, the dynamics of the latter can be neglected $(F_p(z) \approx 1)$. Also, $L(z) \approx 1$ for this analysis. Under these assumptions, (35) has poles at

$$z = \sqrt[N/2]{K_o - K_x} \cdot e^{\pm j2\pi h/(N/2)}, \text{ with } h = 1, 2, \ldots, N/4, \tag{36}$$

which can be better understood if poles are transformed to the continuous-time domain, yielding

$$s = \frac{\log(K_o - K_x)}{(N/2)t_s} \pm j\frac{2\pi h}{(N/2)t_s}, \tag{37}$$

where the pole with the smallest modulus can be calculated by imposing $h = 0$, thus

$$s = \log(K_o - K_x)/(t_s N/2). \tag{38}$$

Fig. 7 (left) shows the modulus of the smallest pole for different values of $(K_o - K_x)$. If $-1 < K_o - K_x < 0$ in (38) the term inside the logarithm becomes negative and the result is a complex number. In this case, the step response has overshoot (see Fig. 7 (right)). If $0 < K_o - K_x < 1$, the response becomes slower and over-damped. If $K_o = K_x$, there is a zero-pole cancellation in (35) and the closed-loop system has a dead-beat behaviour. Therefore, it is clear that the situation of $-1 < K_o - K_x < 0$ should be avoided since both performance and stability margins deteriorate.

## VII. Case Study and Analysis

### A. Case Study

Fig. 8 shows the electrical diagram of the laboratory facilities, while Fig. 9 shows a photograph. The parameters and ratings of hardware components are shown in Table I. DG1 is shown in Fig. 9 (a) and it is connected to the microgrid via an *LCL* filter. The filter parameters are shown in Table I (the same *LCL* filter is used for both VSMs). The parameters in per-unit are $L_i = 0.04$ pu, $C_f = 0.05$ pu, and $L_g = 0.016$ pu. The

| Var. | Value | Var. | Value | Var. | Value |
|---|---|---|---|---|---|
| $L_i$ | 2.3 mH | $S_n$ | 15 kVA | $L_{l2}$ | 5 mH |
| $R_i$ | 0.1 Ω | $V_n$ | 400 V | $R_{l2}$ | 0.2 Ω |
| $L_g$ | 0.9 mH | $f_n$ | 50 Hz | $L_{l3}$ | 2 mH |
| $R_g$ | 0.03 Ω | $V_{dc}$ | 680 V | $R_{l3}$ | 0.1 Ω |
| $C_f$ | 8.8 $\mu$F | $C_{dc}$ | 2 mF | | |

TABLE I
PARAMETERS AND RATINGS OF THE HARDWARE ELEMENTS.

| Var. | Value | Var. | Value | Var. | Value |
|---|---|---|---|---|---|
| $K_p$ | 4.51 | $D_Q$ | 100 | $D_P$ | 20 |
| $K_i$ | $1.21{\cdot}10^3$ | $J_V$ | 0.2 | $K_Q$ | 0.001 |
| $\omega_c$ | 1.5 kHz | $G$ | 5 | $Q$ | 12 |

TABLE II
CONTROL SYSTEM PARAMETERS.

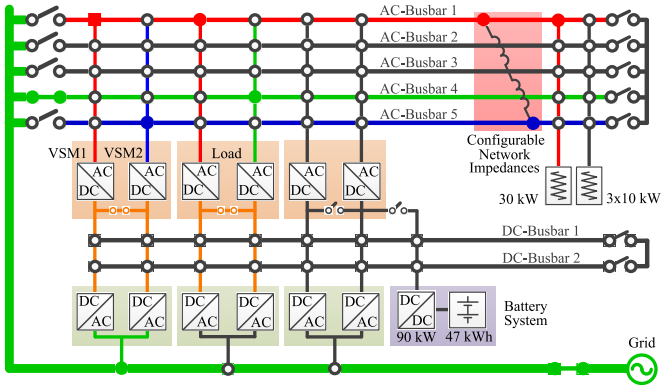


Fig. 8. Electrical diagram of the laboratory. Filled dots indicate an electrical connection. Gray indicate that the bus-bar is not connected.

efficiency of the converter connected to the grid was found to be 95.4 % when operating at full load.

Large output impedances were used for the DGs so that the contribution of the paper was highlighted. DG1 was connected close to the load. Therefore, $L_{g1}$ and $R_{g1}$ were almost zero. VSC2 had the same *LCL* filter, but the line impedance was $L_{g2} = 5$ mH and $R_{g2} = 0.2$ Ω. Fig. 8 shows the electrical single-line diagram of the laboratory facilities. The electrical line was emulated with a set of configurable impedances (see Fig. 9 (b)). DC-link voltages of both converters were maintained constant at 680 V with a diode rectifier and a step-up transformer connected to an auxiliary grid. The total DC-link capacitance was 2 mF. The three-phase diode bridge was emulated with a 15 kW back-to-back converter. An additional configurable linear load was connected in parallel with the non-linear one. All the elements where connected by using the AC and DC bus-bars shown in Fig. 9 (c) and (d), respectively.

The control system parameters are summarised in Table II. Switching and sampling frequencies were configurable, and they were set to 10 kHz. Dead-times of both VSCs were set to 2 $\mu$s. The min-max method was used to generate the PWM signals [53]. Control systems were implemented in embedded PCs (see Fig. 9 (e)) by using an automatic code generation tool. For more details of the laboratory facilities, see [54].


Fig. 9. Photograph of the laboratory facilities. (a) VSC, (b) configurable impedances, (c) AC bus-bars, (d) DC bus-bars, and (e) embedded computers.

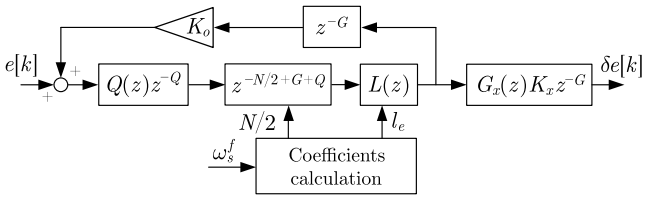


Fig. 10. Implementation of the FGRC. Control blocks are implemented independently.

### B. Control System Design and Implementation

The value of $N$ calculated with (21) is 200. The RC bandwidth has been set to 1500 Hz with a 25th-order linear phase FIR filter ($Q(z)$). The possible values of $K_o$ will be explored in the next Section, while $K_x$ will be set according to (32). The RC was implemented as suggested in [23]. A classical PI ($C(z)$) is used to control the current $i_g$. This controller was designed with a phase margin of 65 deg and a crossover frequency of 200 Hz. Classical decoupling equations are used [53]. The discrete-time version of the continuous-time plant transfer function is obtained by using the ZOH method [55]. Two one-sampling-period delays are added to the model of the plant to model calculations and delays in the measurement chains. Voltage $u_g^f$ used to calculate the fictitious reference current is filtered with a first-order low-pass filter with a cut-off frequency of 150 Hz and a set of notch filters for the harmonics up to the 8th (in *dq*) [44].

Fig. 10 shows the modifications made to the FGRC for its implementation. Some delays ($G$) were taken from $z^{-N}$ to make the transfer function $G_x(z)z^{-G}$ proper. Meanwhile, a number of delays ($Q$) were taken from $z^{-N}$ to make $Q(z)z^{-Q}$ proper as well. The coefficients of the frequency-adaptive filter $L(z)$ were calculated by using a filtered version of the VSM frequency ($\omega_s^f$).

Fig. 11 shows Bode's plot for the open-loop transfer function, which consists of the plant, the FGRC, and the PI current controller. The value of $K_o$ was set to 0.9. The amplification depends on the harmonic number only at low frequencies, while at high frequencies, amplification has a similar value

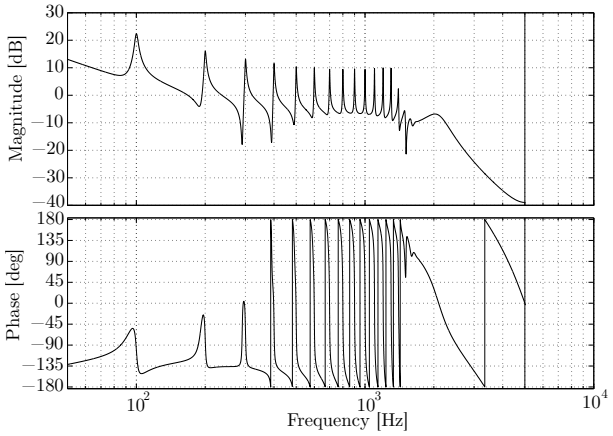


Fig. 11. Bode's plot of the open-loop transfer function including the plant, the FGRC, and the PI current controller.

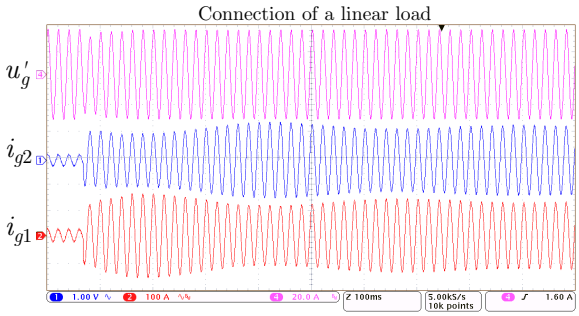


Fig. 12. Operation of the VSM microgrid feeding a linear load. No electrical lines.

for all harmonics. Only the impedance for one harmonic frequency could be adjusted, exactly, as already discussed in Section VI-A.

### C. Practical Design Guide

The following practical design guide has been drawn from the theoretical analysis presented:

1) Design the VSM parameters and the current controller by using any existing method.
2) Obtain $P(z)$. For the case studied in this paper, $P(z)$ is the transfer function of an *LCL* filter in discrete time, including the controller delays (see [56] for more details).
3) Calculate the transfer function of the plant with the current controller $(F_p(z))$ by using (25). If $F_p(z)$ does not have zeros outside the unit circle, $G_x(z)$ can be implemented as shown in (27). Otherwise, an alternative must be used (see [57] for an alternative).
4) Design $Q(z)$ as a zero-phase FIR low-pass filter. Set the filter bandwidth to include the highest harmonic to be dealt with (see [52], Section 5.3.2 for a possible design procedure).
5) Design the value of $R_h$ according to the application requirements (virtual resistance to be inserted at the harmonic frequencies).

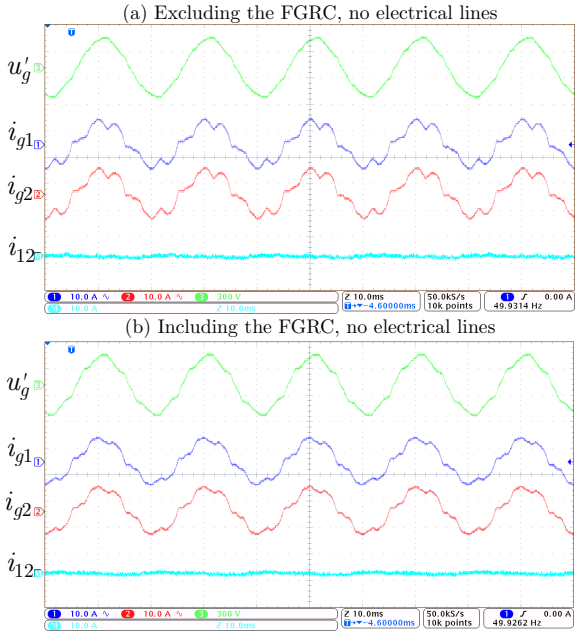


Fig. 13. Operation of the VSM-based microgrid without electrical lines (a) excluding and (b) including the FGRC.

6) Select $K_o$ between 0 and 1. Consider steady-state and transient performance (Sections VI-B and VI-C, respectively).
7) Use (32) to calculate $K_x$ with the values of $K_o$ and $R_h$ from the previous steps. Verify that the stability condition in (29) is satisfied. If it is not, increase the value of $K_o$.
8) If the controller performance deteriorates when the grid frequency changes, include $L(z)$ to provide frequency adaptability (see (22)). Otherwise, $L(z)$ is not necessary.
9) Implement the controller as shown in Fig. 10. Choose $G$ that makes $G_x(z)$ proper. $Q(z)$ is proper if $Q$ delays are moved from $z^{-N/2}$ to $Q(z)$.

## VIII. Experimental Results

*1) Linear load and no electrical lines:* Fig. 12 shows the operation of the VSM-based microgrid feeding a load that consumes only active power. Initially, the load was consuming 1 kW. At a certain point, an 8 kW load was connected and a transient took place. There was a low-frequency oscillation due to the coupling between the VSMs. When the transient finished the load current was shared between the DGs because the droop coefficients of both DGs were the same and there were no electrical lines in between.

*2) Non-Linear Load and no Electrical Lines:* Fig. 13 shows the output current of the VSMs (a) before and (b) after switching the FGRCs on, without electrical lines. The load was non-linear. $K_o = 0.6$. $R_{h'} = 20$, $h' = 11$. $i_{12} = i_{g1} - i_{g2}$. The harmonic sharing was adequate in both cases. Results show, clearly, that impedance equalisation is not required here since the output impedance of both DGs was very similar. In (a), the grid voltage THD was 4.4 %, while in (b) 7.2 %. The current THD was 21.2 % in (a) and 16.5 % in (b).

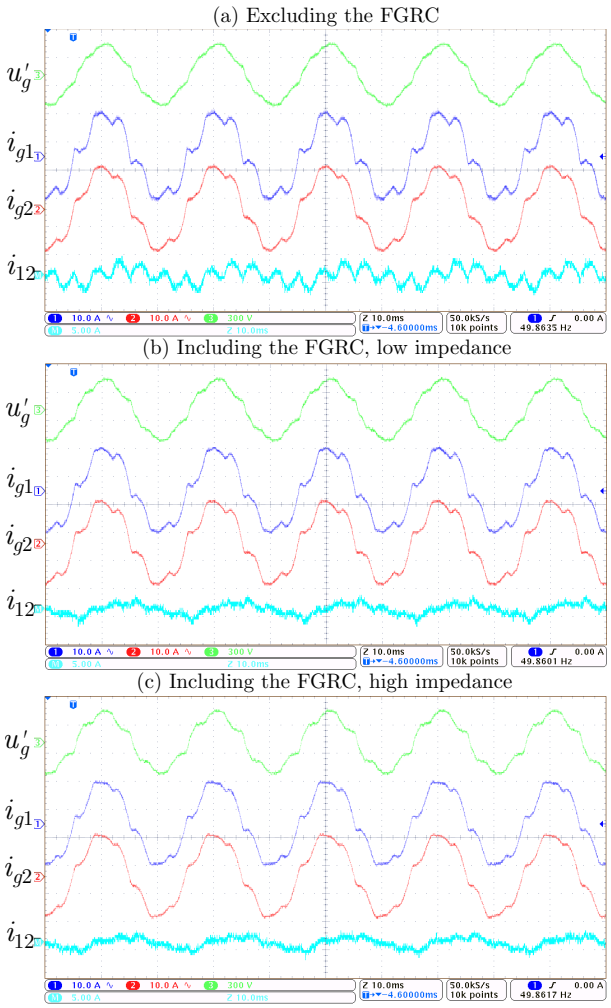


Fig. 14. Operation of the VSM-based microgrid (a) excluding, including the FGRC with (b) low and (c) high impedance.

*3) Non-linear Load and Electrical Lines:* Fig. 14 (a) shows the current harmonic distribution when the FGRCs were excluded. Current harmonics were not equally shared. Fig. 14 (b) shows the same experiment, but the FGRCs were activated. $K_{o1} = 0.65$, $K_{o2} = 0.5$, $R_{h'1} = 20\ \Omega$, $R_{h'2} = 15\ \Omega$, $h' = 11$. Current harmonic sharing improved and waveforms look alike, except for the high frequency components. Also, there was a circulating current of the fundamental frequency between the two converters. This was related to the VSM droop coefficients and the line (not due to the FGRC). In Fig. 14 (c), the value of $R_h$ was increased: $R_{h1} = 30\ \Omega$ and $R_{h2} = 20\ \Omega$. High frequency harmonics were correctly shared. However, the grid voltage THD changed from 7.4 % to 13.1 %, thus highlighting the trade-off between voltage and current quality.

*4) Infinite Gain RC:* Fig. 15 shows the microgrid operation when an classical RC ($K_o = 1$) was applied to DG2. The output current quality greatly improved (the THD was 2.2 %), but the grid voltage was highly distorted (the THD was 10.6 %). All harmonics were delivered to the load by DG1. This situation is undesirable and it is only shown to highlight the need of an FGRC.

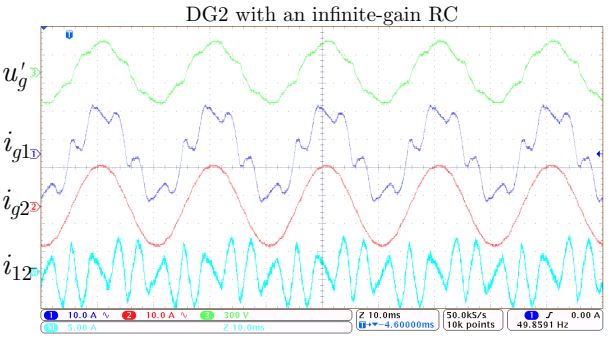


Fig. 15. Operation of the VSM-based microgrid feeding a linear load. A classical RC ($K_o = 1$) is applied to DG2.

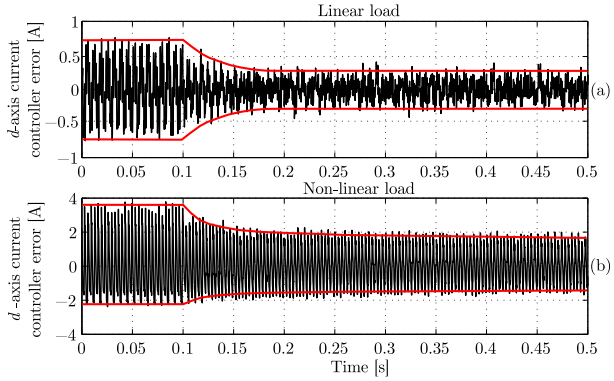


Fig. 16. Transient of $d$-axis current-controller error. $(K_o - K_x) = 0.5$. (a) Linear and (b) non-linear load.

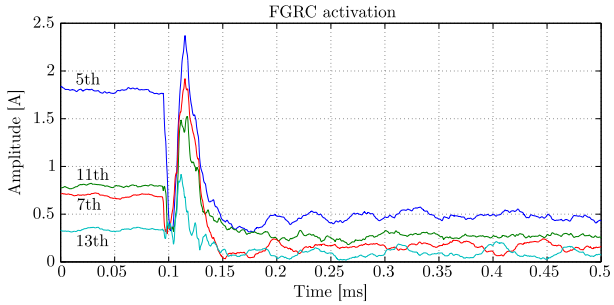


Fig. 17. Harmonic components of $i_{g1} - i_{g2}$ when the FRGCs of both VSMs are turned on. Harmonic number indicated in the figure.

*5) Transient Performance of the RC:* Fig. 16 shows DG1 $d$-axis error for the current controller when the FGRC was switched on (simulation results). $K_o = 0.9$ and $K_x = 0.7$. In Fig. 16 (a), a linear load was used. The dominant pole calculated with (5) was $-69.8$ rad/s and the transient was as expected. In Fig. 16 (b), a non-linear load was connected in parallel with the linear one. Clearly, the transient was slower because the harmonic disturbance was non-linear (depends on the grid voltage), and the system needed more time to reach the steady-state.

Fig. 17 shows the simulation results for the harmonic components of $(i_{g1} - i_{g2})$ when the FGRCs in both VSMs were turned on. Initially, harmonic amplitudes were large. Eventually, differences between them were significantly reduced. However, compensation was not ideal since the proposed

This article has been accepted for publication in a future issue of this journal, but has not been fully edited. Content may change prior to final publication. Citation information: DOI 10.1109/TSG.2019.2913632, IEEE Transactions on Smart Grid



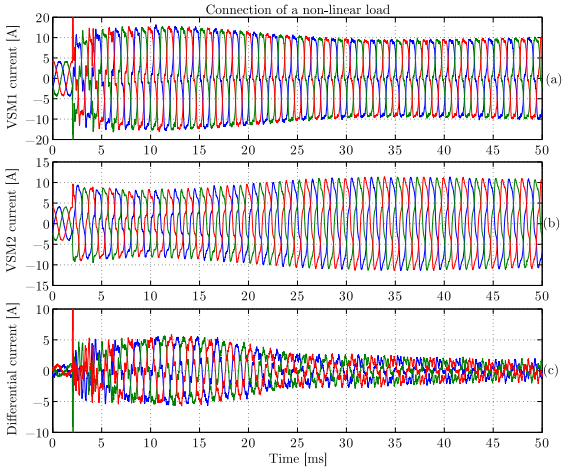


Fig. 18. Connection of the non-linear load (simulation results). (a) VSM1 current, (b) VSM2 current, and (c) differential current.

formulation does not allow independent tuning of harmonic gains.

*6) Connection of Non-Linear Load:* Fig. 18 shows the performance of the VSM microgrid when a non-linear load was connected. Clearly, during the transient current sharing was not accurate. However, after several cycles the system reached the steady state and the current was shared between the two VSMs.

*7) Operation with Three VSMs:* In order to see the performance of the proposed virtual impedance in a more realistic scenario, an additional VSM and an additional load were added to a simulation of the scenario presented in Fig. 1. The electrical single-line diagram is shown in Fig. 19. Parameters of VSM1 and VSM2 were those used previously and the same values were used for VSM3. The virtual impedance values were adjusted by trial and error. However, the development of an optimised design procedure is of interest for further research.

Fig. 20 shows the magnitude of the 5th harmonic consumed by each VSM. Initially, the harmonic was not equally shared: the magnitudes were 2.3 A, 1.2 A, and 2.7 A for the VSMs 1, 2, and 3, respectively. Voltage THDs were 5.9 % and 6.9 %. Eventually, the virtual impedances of all VSMs were turned on and the 5th harmonic was redistributed. After the transient, the harmonic consumption of each VSM was adequate. However, the voltage quality deteriorated because of the virtual impedance effect. It is worth pointing out that large voltage THDs appear because large impedance values were used to model electrical lines.

## IX. Comparative Analysis: Alternative Solutions

In this section, three alternative solutions to the FGRC are presented: 1) resistive virtual impedance, 2) a virtual impedance based on a high-pass filter, and 3) a resonant virtual impedance. Their performance will be critically compared to that of the FGRC.

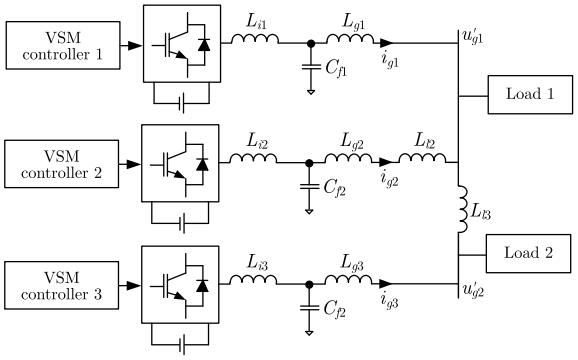


Fig. 19. Electrical single-line diagram for the operation with three VSMs. Each VSM includes an FGRC.

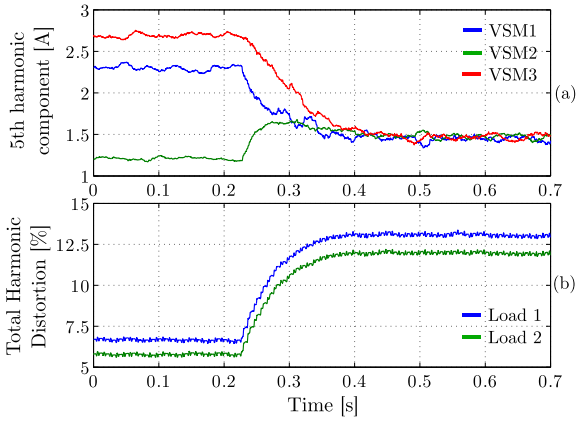


Fig. 20. Operation of the microgrid with three VSMs when the FGRC is turned on. (a) 5th harmonic component and (b) load THDs.

### A. Resistive Virtual Impedance

A common solution for harmonic sharing improvement between converters in parallel connection is the resistive virtual impedance [32]. The transfer function of this method can be written as follows:

$$Z_v^1(z) = R_v, \tag{39}$$

where $R_v$ is the resistive virtual impedance. This solution is simple to design, however, it couples the active- and reactive-power dynamics of the VSM [58]. A simple decoupling system can be implemented in this case. However, it will not be discussed in this paper.

### B. High-Pass Virtual Impedance

A high-pass filter can be added to the conventional implementation of the virtual impedance. This method is known in the literature as transient virtual impedance [32]. This configuration is adequate for VSMs since it does not interact with their low-frequency dynamics. This makes it possible to tune the performance at the harmonic frequencies by using $R_v$ and $L_v$. The discrete-time transfer function of this solution can be written as:

$$Z_v^2(z) = \frac{(z-1)(R_v + j\omega_s L_v)}{z + t_s\omega_{hp} - 1} \tag{40}$$

where $\omega_{hp}$ is the cut-off frequency of the high-pass filter and $L_v$ is the virtual inductance.

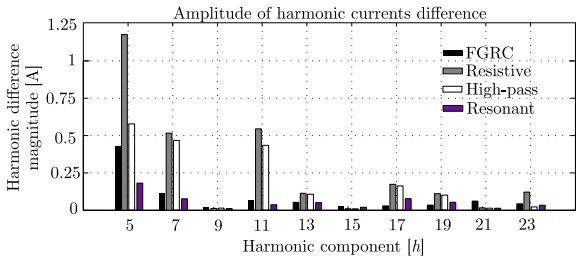


Fig. 21. Amplitude of the harmonic currents, for each one of the solutions tested. (black) FGRC, (grey) resistive, (white) high-pass, and (purple) resonant.

| Alternative: | $THD_1$ | $THD_2$ | $THD_g$ |
|---|---|---|---|
| (a) FGRC | 9.1 % | 13.6 % | 12.0 % |
| (b) Resistive | 20.7 % | 15.6 % | 6.3 % |
| (d) High-pass | 20.3 % | 15.7 % | 6.0 % |
| (c) Resonant | 17.2 % | 15.1 % | 10.2 % |

TABLE III
CURRENT AND GRID VOLTAGE THDS FOR DIFFERENT SOLUTIONS.

### C. Resonant Virtual Impedance

In this method, a finite-gain resonator is added to handle each harmonic, independently. In discrete-time, this transfer function can be written as [8]:

$$Z_v^3(z) = \sum_{h \in \mathrm{H}} Z_v^h(z), \tag{41}$$

where H includes all the harmonics to be addressed, $h$ is the harmonic number and $Z_v^h(z)$ is the transfer function for each harmonic:

$$Z_v^h(z) = R_h \frac{\gamma_h(\alpha_h z + 1)(z-1)}{z^2 - 2a_h \cos(\omega_s h t_s) z + a_h^2}. \tag{42}$$

The virtual resistance is $R_h$, $\alpha_h$ are phase-compensation factors and $\gamma_h$ are normalisation factors. $a_h$ is a damping coefficient. The gain of (42) at the harmonic frequency $h$ is $R_h$. Therefore, the trade-off between current and voltage quality for each harmonic can be independently modified. For the frequency adaptive version of this virtual impedance the coefficient $\cos(\omega_s h t_s)$ should be modified in real time. Resonant virtual impedances up to the 13th harmonic were included here for comparison. The detailed design procedure can be found in [8].

## X. COMPARATIVE ANALYSIS: RESULTS

### A. Harmonic Sharing Performance

Fig. 21 shows the harmonic components obtained for the different solutions, while Table III shows the THDs of the VSM output currents and the grid voltage THD. FGRC clearly reduced the harmonic content, but it did not provide perfect sharing. In addition, due to high impedance present at the harmonic frequencies, the THD of the grid voltage increased. The resistive virtual impedance was not useful to redistribute current harmonics because the impedance of the line that interconnects the VSM2 with the load is large. For the high-pass filter, the results clearly improved, especially for the 5th harmonic. Finally, the resonant virtual impedances gave the best results. However, the gain of each resonant controller needed to be adjusted by trial and error until accurate sharing was achieved.

| Alternative: | Mult. | Adds | Mem. | Trig. |
|---|---|---|---|---|
| (a) FGRC | 48 | 53 | 244 | 0 |
| (b) Resistive | 2 | 4 | 0 | 0 |
| (d) High-pass | 8 | 10 | 4 | 0 |
| (c) Resonant | 84 | 72 | 24 | 12 |

TABLE IV
COMPUTATIONAL COMPLEXITY OF THE ALTERNATIVES.

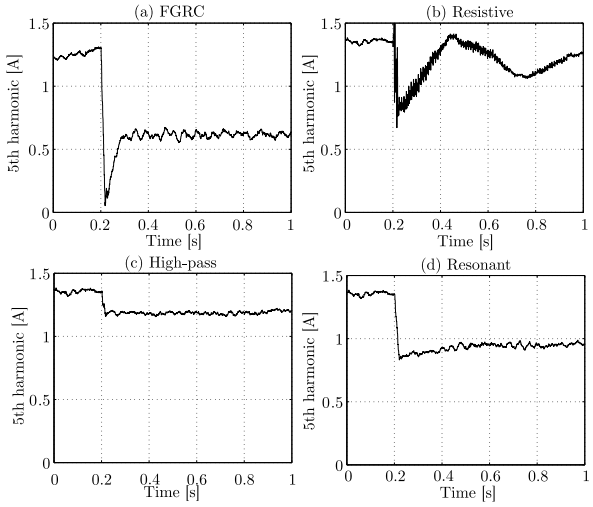


Fig. 22. Transient performance (simulation) of different virtual impedance solutions tested. (a) FGRC, (b) resistive, (c) high-pass, and (d) resonant virtual impedance.

### B. Transient Performance

Fig. 22 shows the transient performance of the 5th harmonic of the output current when the different solutions were activated. The transient of the FGRC was fast, and it had overshoot. The transient of the resistive virtual impedance was slow and damping was not adequate because the resistive virtual impedance couples the dynamics of the VSM and the harmonics. This coupling effect disappeared for the high-pass virtual impedance. Finally, the transient performance of the resonant virtual impedances was fast and well damped.

### C. Computational Complexity

Table IV illustrates the computational complexity of the virtual impedance solutions used in the comparative analysis. The resistive and the high-pass solutions are the most efficient ones. FRGC requires a large amount of storage, but less calculations than the resonant virtual impedances. In addition, no trigonometric functions are required in the former. The computational complexity of FGRC can be reduced if the order of the filter $Q(z)$ is reduced. The computational complexity of the resonant virtual impedances is directly related to number of harmonics addressed. In fact, for a reduced number of harmonics it can be an efficient solution.

## XI. Conclusion

In this paper, a RC with a finite gain at the harmonic frequencies (FGRC) has been proposed to improve current harmonic sharing in VSM-based microgrids. Similarity and comparison between a current-controlled VSM and a conventional VSM with virtual impedance application have been drawn. The main conclusions of this work are summarised below:

1) An FGRC inside a current controller can be used to shape the output impedance of a VSM for harmonic frequencies.
2) The Virtual harmonic resistance $(R_h)$ of an FRGC can be designed only for one specific harmonic. However, it has been shown that harmonic current sharing can be significantly improved if this value is chosen carefully.
3) Robustness against frequency variations can be improved by designing $K_o$ carefully. Furthermore, when changing $K_o$ was insufficient to deal with variable frequency conditions, an adaptive filter added to the FGRC guaranteed frequency adaptability.
4) The comparative analysis revealed that FGRC exhibits better steady-state performance than resistive and high-pass virtual impedances. The best results were obtained when resonant virtual impedances were used, but it was necessary to adjust all the controller gains.
5) Resistive and high-pass virtual impedance methods were, both, computationally efficient. While, FGRC had less computational complexity than resonant virtual impedances, but it required more memory storage.
6) This paper considered resistive harmonic virtual impedances, only. However, it would be of interest to evaluate the effect of an inductive part and find a method to optimise resistance and inductance design.

## References


[1] J. Guerrero, M. Chandorkar, T. Lee, and P. Loh, "Advanced control architectures for intelligent microgrids-Part I: decentralized and hierarchical control," *IEEE Trans. on Ind. Elec.*, vol. 60, no. 4, pp. 1254–1262, April 2013.

[2] Q. C. Zhong, "Power-electronics-enabled autonomous power systems: Architecture and technical routes," *IEEE Trans. on Ind. Elec.*, vol. 64, no. 7, pp. 5907–5918, July 2017.

[3] S. D'Arco and J. A. Suul, "Equivalence of virtual synchronous machines and frequency-droops for converter-based microgrids," *IEEE Trans. on Smart Grid*, vol. 5, no. 1, pp. 394–395, Jan 2014.

[4] H. Wu, X. Ruan, D. Yang, X. Chen, W. Zhao, Z. Lv, and Q. C. Zhong, "Small-signal modeling and parameters design for virtual synchronous generators," *IEEE Trans. on Ind. Elec.*, vol. 63, no. 7, pp. 4292–4303, July 2016.

[5] Q. C. Zhong and G. Weiss, "Synchronverters: Inverters that mimic synchronous generators," *IEEE Trans. on Ind. Elec.*, vol. 58, no. 4, pp. 1259–1267, April 2011.

[6] O. Mo, S. D'Arco, and J. A. Suul, "Evaluation of virtual synchronous machines with dynamic or quasi-stationary machine models," *IEEE Trans. on Ind. Elec.*, vol. PP, no. 99, pp. 1–1, 2016.

[7] Z. Shuai, W. Huang, C. Shen, J. Ge, and Z. J. Shen, "Characteristics and restraining method of fast transient inrush fault currents in synchronverters," *IEEE Trans. on Ind. Elec.*, vol. 64, no. 9, pp. 7487–7497, Sept 2017.

[8] J. Roldan-Perez, A. Rodriguez-Cabero, and M. Prodanovic, "Harmonic virtual impedance design for parallel-connected grid-tied synchronverters," *IEEE Journal of Emerging and Selected Topics in Power Electronics*, vol. 7, no. 1, pp. 493–503, March 2018.

[9] Y. Hirase, K. Sugimoto, K. Sakimoto, and T. Ise, "Analysis of resonance in microgrids and effects of system frequency stabilization using a virtual synchronous generator," *IEEE Journal of Emerging and Selected Topics in Power Electronics*, vol. 4, no. 4, pp. 1287–1298, Dec 2016.

[10] T. Younis, M. Ismeil, E. K. Hussain, and M. Orabi, "Single-phase self-synchronized synchronverter with current-limiting capability," in *2016 Eighteenth International Middle East Power Systems Conference (MEPCON)*, Dec 2016, pp. 848–853.

[11] K. Sakimoto, K. Sugimoto, and Y. Shindo, "Low voltage ride through capability of a grid connected inverter based on the virtual synchronous generator," in *2013 IEEE 10th International Conference on Power Electronics and Drive Systems (PEDS)*, April 2013, pp. 1066–1071.

[12] Y. Chen, R. Hesse, D. Turschner, and H. Beck, "Improving the grid power quality using virtual synchronous machines," in *2011 International Conference on Power Engineering, Energy and Electrical Drives*, May 2011, pp. 1–6.

[13] W. Zhang, A. M. Cantarellas, J. Rocabert, A. Luna, and P. Rodriguez, "Synchronous power controller with flexible droop characteristics for renewable power generation systems," *IEEE Transactions on Sustainable Energy*, vol. 7, no. 4, pp. 1572–1582, Oct 2016.

[14] M. Reyes, P. Rodriguez, S. Vazquez, A. Luna, R. Teodorescu, and J. M. Carrasco, "Enhanced decoupled double synchronous reference frame current controller for unbalanced grid-voltage conditions," *IEEE Transactions on Power Electronics*, vol. 27, no. 9, pp. 3934–3943, Sept 2012.

[15] D. Remon, A. M. Cantarellas, J. M. Mauricio, and P. Rodriguez, "Power system stability analysis under increasing penetration of photovoltaic power plants with synchronous power controllers," *IET Renewable Power Generation*, vol. 11, no. 6, pp. 733–741, 2017.

[16] P. Rodrguez, C. Citro, J. I. Candela, J. Rocabert, and A. Luna, "Flexible grid connection and islanding of spc-based pv power converters," *IEEE Transactions on Industry Applications*, vol. 54, no. 3, pp. 2690–2702, May 2018.

[17] V. Natarajan and G. Weiss, "Synchronverters with better stability due to virtual inductors, virtual capacitors, and anti-windup," *IEEE Trans. on Ind. Elec.*, vol. 64, no. 7, pp. 5994–6004, July 2017.

[18] J. Roldán-Pérez, M. Prodanovic, and A. Rodríguez-Cabero, "Parallel current-controlled synchronverters for voltage and frequency regulation in weak grids," in *9th International Conference on Pow. Elec., Machines and Drives (under evaluation)*, November 2018.

[19] J. He, Y. W. Li, F. Blaabjerg, and X. Wang, "Active harmonic filtering using current-controlled, grid-connected dg units with closed-loop power control," *IEEE Trans. on Pow. Elec.*, vol. 29, no. 2, pp. 642–653, Feb 2014.

[20] J. He and Y. W. Li, "Analysis, design, and implementation of virtual impedance for power electronics interfaced distributed generation," *IEEE Trans. on Ind. App.*, vol. 47, no. 6, pp. 2525–2538, Nov 2011.

[21] A. García-Cerrada, O. Pinzón-Ardila, V. Feliu-Batlle, P. Roncero-Sánchez, and P. García-Gonzalez, "Application of a repetitive controller for a three-phase active power filter," *IEEE Trans. on Pow. Elec.*, vol. 22, no. 1, pp. 237–246, 2007.

[22] D. Chen, J. Zhang, and Z. Qian, "Research on fast transient and $6n\pm1$ harmonics suppressing repetitive control scheme for three-phase grid-connected inverters," *IET Pow. Elec.*, vol. 6, no. 3, pp. 601–610, 2013.

[23] J. Roldán-Pérez, A. García-Cerrada, J. L. Zamora-Macho, P. Roncero-Sánchez, and E. Acha, "Troubleshooting a digital repetitive controller for a versatile dynamic voltage restorer," *International Journal of Electrical Power & Energy Systems*, vol. 57, no. 0, pp. 105–115, 2014.

[24] G. Escobar, M. Hernandez-Gomez, A. A. Valdez-Fernandez, M. J. Lopez-Sanchez, and G. A. Catzin-Contreras, "Implementation of a $6n\pm1$ repetitive controller subject to fractional delays," *IEEE Trans. on Ind. Elec.*, vol. 62, no. 1, pp. 444–452, Jan 2015.

[25] Z. X. Zou, K. Zhou, Z. Wang, and M. Cheng, "Frequency-adaptive fractional-order repetitive control of shunt active power filters," *IEEE Trans. on Ind. Elec.*, vol. 62, no. 3, pp. 1659–1668, March 2015.

[26] P. Prasitmeeboon, "Design of repetitive controller using optimization in frequency domain with maximum gain constraints," in *2018 9th International Conference on Mechanical and Aerospace Engineering (ICMAE)*, July 2018, pp. 204–207.

[27] R. E. Torres-Olguin, G. Escobar, A. A. Valdez, and P. G. Hernandez-Briones, "A modified repetitive-based controller for an active filter to compensate harmonics 6k+1," in *2008 IEEE Power Electronics Specialists Conference*, June 2008, pp. 4650–4655.

[28] G. Escobar, P. Mattavelli, M. Hernandez-Gomez, and P. R. Martinez-Rodriguez, "Filters with linear-phase properties for repetitive feedback," *IEEE Transactions on Industrial Electronics*, vol. 61, no. 1, pp. 405–413, Jan 2014.

[29] J. Roldán-Pérez, M. Prodanovic, A. Rodríguez-Cabero, J. Guerrero, and A. García-Cerrada, "Finite-gain current repetitive controller for synchronverters with harmonic sharing capabilities," in *International Conference on Harmonic and Quality of Power (ICHQP 2018)*, 2018.
[30] U. Borup, F. Blaabjerg, and P. N. Enjeti, "Sharing of nonlinear load in parallel-connected three-phase converters," *IEEE Transactions on Industry Applications*, vol. 37, no. 6, pp. 1817–1823, Nov 2001.
[31] S. J. Chiang, C. Y. Yen, and K. T. Chang, "A multimodule parallelable series-connected pwm voltage regulator," *IEEE Transactions on Industrial Electronics*, vol. 48, no. 3, pp. 506–516, June 2001.
[32] X. Wang, Y. W. Li, F. Blaabjerg, and P. C. Loh, "Virtual-impedance-based control for voltage-source and current-source converters," *IEEE Transactions on Power Electronics*, vol. 30, no. 12, pp. 7019–7037, Dec 2015.
[33] W. Yao, M. Chen, J. Matas, J. M. Guerrero, and Z. M. Qian, "Design and analysis of the droop control method for parallel inverters considering the impact of the complex impedance on the power sharing," *IEEE Trans. on Ind. Elec.*, vol. 58, no. 2, pp. 576–588, Feb 2011.
[34] S. Munir and Y. W. Li, "Residential distribution system harmonic compensation using pv interfacing inverter," *IEEE Trans. on Smart Grid*, vol. 4, no. 2, pp. 816–827, June 2013.
[35] X. Chen, X. Ruan, D. Yang, W. Zhao, and L. Jia, "Injected grid current quality improvement for a voltage-controlled grid-connected inverter," *IEEE Trans. on Pow. Elec.*, vol. 33, no. 2, pp. 1247–1258, Feb 2018.
[36] C. Blanco, D. Reigosa, J. C. Vasquez, J. M. Guerrero, and F. Briz, "Virtual admittance loop for voltage harmonic compensation in microgrids," *IEEE Trans. on Ind. App.*, vol. 52, no. 4, pp. 3348–3356, July 2016.
[37] D. De and V. Ramanarayanan, "Decentralized parallel operation of inverters sharing unbalanced and nonlinear loads," *IEEE Transactions on Power Electronics*, vol. 25, no. 12, pp. 3015–3025, Dec 2010.
[38] A. D. Paquette and D. M. Divan, "Virtual impedance current limiting for inverters in microgrids with synchronous generators," *IEEE Transactions on Industry Applications*, vol. 51, no. 2, pp. 1630–1638, March 2015.
[39] J. He, L. Du, B. Liang, Y. Li, and C. Wang, "Coupled-virtual-impedance control for ac/dc hybrid microgrid power electronic interlinking unit with dual converters," *IEEE Trans. on Smart Grid*, pp. 1–1, 2018.
[40] X. Wang, F. Blaabjerg, and Z. Chen, "Autonomous control of inverter-interfaced distributed generation units for harmonic current filtering and resonance damping in an islanded microgrid," *IEEE Transactions on Industry Applications*, vol. 50, no. 1, pp. 452–461, Jan 2014.
[41] R. Ni, Y. W. Li, Y. Zhang, N. R. Zargari, and Z. Cheng, "Virtual impedance-based selective harmonic compensation (vi-shc) pwm for current source rectifiers," *IEEE Trans. on Pow. Elec.*, vol. 29, no. 7, pp. 3346–3356, July 2014.
[42] J. He, Y. W. Li, and M. S. Munir, "A flexible harmonic control approach through voltage-controlled dggrid interfacing converters," *IEEE Transactions on Industrial Electronics*, vol. 59, no. 1, pp. 444–455, Jan 2012.
[43] H. Tian, Y. W. Li, and P. Wang, "Hybrid ac/dc system harmonics control through grid interfacing converters with low switching frequency," *IEEE Trans. on Ind. Elec.*, vol. 65, no. 3, pp. 2256–2267, March 2018.
[44] J. Roldán-Pérez, A. Rodríguez-Cabero, and M. Prodanovic, "Harmonic virtual impedance design for a synchronverter-based battery interface converter," in *6th International Conference on Renewable Energy Research and Applications*, November 2017.
[45] M. Savaghebi, A. Jalilian, J. Vasquez, and J. Guerrero, "Secondary control scheme for voltage unbalance compensation in an islanded droop-controlled microgrid," *IEEE Trans. on Smart Grid*, vol. 3, no. 2, pp. 797–807, June 2012.
[46] L. Meng and J. M. Guerrero, "Optimization for customized power quality service in multibus microgrids," *IEEE Trans. on Ind. Elec.*, vol. 64, no. 11, pp. 8767–8777, Nov 2017.
[47] J. Roldán-Pérez, M. Prodanovic, and A. Rodríguez-Cabero, "Detailed discrete-time implementation of a battery-supported synchronverter for weak grids," in *43nd Annual Conference of the IEEE Ind. Elec. Society (IECON)*, 2017.
[48] S. Dong and Y. C. Chen, "A method to directly compute synchronverter parameters for desired dynamic response," *IEEE Trans. on Ene. Conv.*, vol. 33, no. 2, pp. 814–825, June 2018.
[49] H. Akagi, E. H. Watanabe, and M. Aredes, *Instantaneous Power Theory and Applications to Power Conditioning*. Wiley, 2007.
[50] J. Olm, G. Ramos, and R. Costa-Castelló, "Stability analysis of digital repetitive control systems under time-varying sampling period," *IET Control Theory Applications*, vol. 5, no. 1, pp. 29–37, 2011.
[51] K. Zhou and D. Wang, "Digital repetitive learning controller for three-phase CVCF PWM inverter," *IEEE Trans. on Ind. Elec.*, vol. 48, pp. 820–830, 2001.
[52] R. G. Lyons, *Understanding digital signal processing*. Addison Wesley Pub. Co Reading, Mass, 1997.
[53] A. Yazdani and R. Iravani, *Voltage-Sourced Converters in Power Systems*. Wiley, 2010.
[54] F. Huerta, J. K. Gruber, M. Prodanovic, and P. Matatagui, "Power-hardware-in-the-loop test beds: evaluation tools for grid integration of distributed energy resources," *IEEE Ind. App. Magazine*, vol. 22, no. 2, pp. 18–26, March 2016.
[55] B. Kuo, *Automatic control system*. Prentice-Hall International London, 1962.
[56] J. Roldán-Pérez, E. J. Bueno, R. Peña-Alzola, and A. Rodríguez-Cabero, "All-pass-filter-based active damping for vscs with lcl filters connected to weak grids," *IEEE Trans. on Pow. Elec.*, vol. 33, no. 11, pp. 9890–9901, Nov 2018.
[57] M. Tomizuka, "Zero phase error tracking algorithm for digital control," *Journal of Dynamic Systems, Measurement, and Control*, vol. 109, no. 1, pp. 65–68, 1987.
[58] H. Wu, X. Ruan, D. Yang, X. Chen, W. Zhao, Z. Lv, and Q. Zhong, "Small-signal modeling and parameters design for virtual synchronous generators," *IEEE Transactions on Industrial Electronics*, vol. 63, no. 7, pp. 4292–4303, July 2016.

**Javier Roldán-Pérez** (S'12-M'14) received a B.S. degree in industrial engineering, a M.S. degree in electronics and control systems, a M.S. degree in system modeling, and a Ph.D. degree in power electronics, all from Comillas Pontifical University, Madrid, in 2009, 2010, 2011, and 2015, respectively. From 2010 to 2015, he was with the Institute for Research in Technology (IIT), Comillas University. In 2014, he was a visiting Ph.D. student at the Department of Energy Technology, Aalborg University, Denmark. From 2015 to 2016 he was with the Electric and Control Systems Department at Norvento Distributed Energy. In September 2016 he joined the Electrical Systems Unit at IMDEA Energy Institute, where his research topics are the integration of renewable energies, microgrids, and power electronics applications.

**Milan Prodanovic** (M'01) received the B.Sc. degree in electrical engineering from the University of Belgrade, Serbia, in 1996 and the Ph.D. degree from Imperial College, London, U.K., in 2004. From 1997 to 1999 he was with GVS engineering company, Serbia, developing UPS systems. From 1999 until 2010 he was a research associate in Electrical and Electronic Engineering at Imperial College, London, UK. Currently he is a Senior Researcher and Head of the Electrical Systems Unit at Institute IMDEA Energy, Madrid, Spain. His research interests include design and control of power electronics interfaces for distributed generation, micro-grids control and active management of distribution networks.

**Alberto Rodríguez-Cabero** obtained his degrees in Industrial Technical Engineering and Industrial Engineering specialized in Electronics in 2011 and 2013, respectively, both from Comillas Pontifical University. In 2016, he obtained the Master in Research in Engineering Systems Modelling in the same University. From 2014 to 2015, he worked as control engineer at Institute for Research in Technology (IIT), Comillas Pontifical University, Madrid. Since September 2015 he is working in the Electrical Systems Unit, Institute IMDEA Energy, Madrid. His areas of interest include the design and control of power electronics converters, power quality and micro-grids.

**Josep M. Guerrero** (S'01-M'04-SM'08-FM'15) received the B.S. degree in telecommunications engineering, the M.S. degree in electronics engineering, and the Ph.D. degree in power electronics from the Technical University of Catalonia, Barcelona, in 1997, 2000 and 2003, respectively. Since 2011, he has been a Full Professor with the Department of Energy Technology, Aalborg University, Denmark, where he is responsible for the Microgrid Research Program (www.microgrids.et.aau.dk). From 2014 he is chair Professor in Shandong University; from 2015 he is a distinguished guest Professor in Hunan University; and from 2016 he is a visiting professor fellow at Aston University, UK, and a guest Professor at the Nanjing University of Posts and Telecommunications. From 2019 he became a Villum Investigator.

His research interests is oriented to different microgrid aspects, including power electronics, distributed energy-storage systems, hierarchical and cooperative control, energy management systems, smart metering and the internet of things for AC/DC microgrid clusters and islanded minigrids; recently specially focused on maritime microgrids for electrical ships, vessels, ferries and seaports. Prof. Guerrero is an Associate Editor for a number of IEEE TRANSACTIONS. He has published more than 500 journal papers in the fields of microgrids and renewable energy systems, which are cited more than 30,000 times. He received the best paper award of the IEEE Transactions on Energy Conversion for the period 2014-2015, and the best paper prize of IEEE-PES in 2015. As well, he received the best paper award of the Journal of Power Electronics in 2016. During five consecutive years, from 2014 to 2018, he was awarded by Clarivate Analytics (former Thomson Reuters) as Highly Cited Researcher. In 2015 he was elevated as IEEE Fellow for his contributions on distributed power systems and microgrids.

**A. García-Cerrada** (M'91-SM'15) obtained his Electrical Engineering degree from Universidad Politécnica de Madrid (Spain) in 1986 and his Ph. D. degree (Electronic and Electrical Engineering) from The University of Birmingham (U.K.) in 1991. He is a Professor of the Electronics, Control Engineering and Communications Department and a member of the staff of the Institute for Research in Technology (IIT) in the ICAI School of Engineering (Universidad Pontificia Comillas) in Madrid (Spain). His research interests include electrical drive control, power electronics applications in electric energy systems (FACTS and Custom Power) and control applications for switched power converters. He is a senior member of IEEE and a member of IET.